W-Band Pulse Generation Using Phase-Locked Lasers and High-Power Photodiode

Victoria A. Carey, Matthew R. Konkol, Charles E. Harrity, Eliezer L. Shahid, Christopher A. Schuetz, Peng Yao, and Dennis W. Prather, *Fellow, IEEE*

***Abstract*— We present an RF photonic pulse generator operating at 77 GHz that can be implemented with multioctave RF tunability. Capitalizing on the beat frequency provided by an optical heterodyne, optical pulse generation is achieved using a low-speed, null-biased Mach-Zehnder modulator while RF pulse generation is achieved using a high-speed, high-power photodiode. Peak photodiode output power as high as 27.4 dBm is reported with a pulse width of 5 ns and a pulse repetition frequency of 1 MHz. System architecture is described, and photodiode output power as a function of duty cycle is investigated.**

***Index Terms*— Millimeter wave generation, photodiode, pulse generation, radar.**

I. Introduction

RADIO detection and ranging, commonly radar, has been in perpetual development since its inception. Using the echo of a transmitted signal to derive information about the (unseen) environment is a powerful tool and one that is leveraged in a multitude of applications. A fairly recent and widespread application is that of anti-collision automotive radar, where fine range resolution and detection ranges spanning 0.15-250 m are desirable [1]. The former has motivated a shift in operational frequencies, or carriers, from K-band (24 GHz) to W-band (77 GHz) following the inverse dependence of range resolution on bandwidth.

This relationship between increased bandwidth and finer range resolution has also inspired photonic solutions where optical channels can be leveraged for real-time bandwidths spanning THz [2]. Although THz bandwidths have not yet been demonstrated, 30 GHz bandwidth and 3.9 mm range resolution, with the added benefit of continuous W-band tunability, has been demonstrated using linear frequency-modulated continuous-wave (FWCW) photonic radar [3]. However, despite the inclusion of a W-band power amplifier, the implementation in [3] was limited to a detection range of 6 m.

Achieved detection range depends on several system and environmental factors which can be represented by a simplified expression of the radar range equation [4]:

$$R_{max} = \sqrt[4]{\frac{P_t G A_e \sigma}{(4\pi)^2 S_n B_n F_n (\frac{S}{N})_{min}}}, \tag{1}$$

where P_t is the peak transmit power, G is the transmit antenna gain, A_e is the receive antenna effective aperture, σ is the radar cross section of the target, S_n is the receive noise power spectral density, B_n is the noise bandwidth, commonly approximated as the signal bandwidth, F_n is the receive noise figure, and $(\frac{S}{N})_{min}$ is the minimum signal-to-noise ratio for detection. For illustrative purposes, Table I gives a set of metrics for a radar system that includes values found in literature and an expected signal bandwidth for the 5 ns minimum pulse width demonstrated in this work. Using Eq. (1), the values in Table I, and the 27.4 dBm peak power achieved in this work, the expected maximum detection range is 300 m, which exceeds the desired range for automotive radar. To the best of our knowledge, 27.4 dBm is the highest reported peak power for an RF photonic pulse generator operating at W-band, and, unlike in [3], is generated without an RF amplifier.

TABLE I
ILLUSTRATIVE RADAR SYSTEM METRICS

G (dB)	A_e (m^2)	σ (m^2)	S_n (dBW/Hz)	B_n (MHz)	F_n (dB)	$(\frac{S}{N})_{min}$ (dB)
24.8 [5]	0.5 [5]	1 [4]	-114 [4]	200	8 [6]	10 [1]

In addition to maximum range, the expected minimum range (and range resolution) is 0.75 m given a 5 ns pulse width, and the expected maximum unambiguous range is 150 m given a 1 μs pulse period. Although these metrics are only viable for mid-range automotive radar [1], they do not represent fundamental limitations of the approach. Shorter pulse widths and longer pulse periods are supported [7], [8] that would satisfy short- and long-range radars, respectively.

The ability of the photonic system presented to achieve W-band peak powers >20 dBm without RF amplification is inherent to pulsed-wave (PW) operation circumventing thermal limitations present in CW operation. Specifically, the transmit power of an RF photonic system relies on the performance of the downconversion module preceding the antenna, namely the photodiode (PD). Spanning the last two decades, PDs have seen continual improvement in power generation following the prolific uni-travelling-carrier (UTC) structure and derivatives thereof that enable coincident high-speed and high-power PD design [9]. Although the UTC structure has enabled PD power generation in CW operation to exceed 10 dBm through W-band [10] and 30 dBm through X-band [11],

Manuscript received April 11, 2022; revised May 19, 2022; accepted May 23, 2022. Date of publication May 27, 2022; date of current version June 6, 2022. This work was supported in part by the U.S. Air Force Research Laboratory under Contract FA8650-19-C-1027. *(Corresponding author: Victoria A. Carey.)*

Victoria A. Carey and Dennis W. Prather are with the Electrical and Computer Engineering Department, University of Delaware, Newark, DE 19716 USA, and also with Phase Sensitive Innovations Inc., Newark, DE 19713 USA (e-mail: vcarey@udel.edu).

Matthew R. Konkol, Charles E. Harrity, Eliezer L. Shahid, Christopher A. Schuetz, and Peng Yao are with Phase Sensitive Innovations Inc., Newark, DE 19713 USA.

Color versions of one or more figures in this letter are available at https://doi.org/10.1109/LPT.2022.3178628.

Digital Object Identifier 10.1109/LPT.2022.3178628

it has been shown that PW operation can mitigate thermal runaway and improve PD performance further. Peak PD power generation exceeding 40 dBm for X- through K-band has been demonstrated using a single-laser RF photonic pulse generation system [7], [8] that would be well-suited for radar applications. The work presented here builds upon this work by (1) extending the investigation of improved PD power during PW operation to W-band and (2) presenting an alternative RF pulse generation system that uses a two-laser optical heterodyne approach.

The use of an optical heterodyne hosts several advantages in comparison with the external modulation approach. First, the RF generation is shifted from the electrical domain to the optical domain by generating the desired RF at the PD directly via an optical beat frequency. This reduces the performance requirements of the RF oscillator and EO phase modulator, at the cost of a second laser. Second, shifting the RF generation to the optical domain also shifts the RF tuning to the optical domain, which is executed by thermal tuning of the lasers and can span multiple octaves of RF bandwidth. Third, the conversion loss in the modulator is avoided, which supports future systems that may benefit from excluding optical amplification.

A similar two-laser approach for W-band pulse generation has been presented elsewhere but with the optical pulse formed by sweeping the bias voltage on the PD rather than using a modulator [12]. The advantage of using a modulator is that the pulse shape is decoupled from the power generation of the PD. In [12], the pulse width and extinction varies with photocurrent, bias condition, and subsequent power output. As a result, maintaining the desired pulse shape while also increasing transmit power is difficult and would be undesirable for a radar system operating according to Eq. (1). In contrast, the system presented here allows independent control of pulse shape and peak transmit power, while preserving the benefits of an optical heterodyne.

II. Theory of Operation

The pulse generation system used here can be described in three parts: optical phase locking using a tunable optically paired source (TOPS) [13], optical pulse generation using a low-speed, null-biased Mach-Zehnder modulator (MZM), and RF pulse generation using a high-speed, high-power PD, as shown graphically in Fig. 1. From left to right along Fig. 1, two optical tones are generated by two lasers, which will be referred to as the reference laser (f_{ref}) and the tune laser (f_{tun}). Next, an RF tone is generated by a phase-locked local oscillator (LO) and input to an amplifier. The amplifier is driven to saturation, generating a frequency comb of the LO that is then upconverted as sidebands of the reference laser by an EO phase modulator. The comb includes harmonics at integer multiples of the LO that can be selected by an optical filter, which dictates the resultant RF carrier. In the measurements that follow, the LO is set to 19.25 GHz and the fourth harmonic is selected for an RF carrier of 77 GHz. Once the desired sideband is selected by the optical filter, it is *injected* into the tune laser with a circulator. When f_{tun} is near the frequency of the injected sideband, which is achieved by thermal tuning, it will *lock* to this sideband, resulting in a pair of phase-locked lasers. For an extensive treatment of the TOPS, the reader is referred to [13]. Neglecting phase variations and assuming pure sinusoidal tones, the time-varying output from the TOPS can be expressed mathematically as:

$$E_{inc} \propto \sqrt{P_{ref}}\cos(2\pi f_{ref} t) + \sqrt{P_{tun}}\cos(2\pi f_{tun} t), \quad (2)$$

where P_{ref} and P_{tun} are the laser powers, and f_{ref} and f_{tun} are the laser frequencies. Figure 1 (a) illustrates (2) in both time and frequency.

After the TOPS, the signal enters the optical pulse generator where it passes through an MZM and becomes time-gated. In this case, the gating occurs due to MZM operation at null bias paired with a square wave, or pulse train, with low and high voltage levels set to V_{null} and $V_{\pi} + V_{null}$, respectively. This results in a swing between null bias and peak bias at the onset of each pulse. Since null bias is the destructive interference condition for the MZM (*off*), and peak bias is the constructive interference condition (*on*), the swing between the two performs a switching operation, effectively gating the optical signal in time. The pulse train is generated by a digital delay (Highland T564) and fed into a modulator driver that also takes instruction from a bias controller to ensure correct voltage levels. For brevity, the modulator driver and bias controller are not pictured in Fig. 1. The resulting time-varying gate signal can be expressed using a Fourier series as:

$$G \propto \delta\Big(1 + 2\sum_{n=1}^{N}\mathrm{sinc}(n\delta)\cos(\frac{2\pi n}{T}t)\Big), \quad (3)$$

where δ is the duty cycle ($\delta = \tau/T$), τ is the pulse width, and T is the pulse period. Figure 1 (b) illustrates the product of (2) and (3) in both time and frequency.

Following the MZM, the signal passes through an erbium-doped fiber amplifier and variable optical attenuator before entering the RF pulse generator where it is focused onto a PD. The RF output from the PD is accessed with a ground-signal-ground coplanar waveguide probe, through which the applied bias is also delivered to the PD. This signal path is enabled via bias tee as illustrated in Fig. 1. After the PD, the PW photocurrent follows the incident optical signal as:

$$I_{ph} = \Re H P_{inc} \propto \Re H G E_{inc}^2, \quad (4)$$

where $\Re$ is the average PD responsivity in amperes per watt, and H is a dimensionless quantity that describes the frequency response. Expanding the square and simplifying gives:

$$I_{ph} \propto \Re H G\left[\frac{P_{ref} + P_{tun}}{2} + \sqrt{P_{ref}P_{tun}}\cos(2\pi f_{rf} t)\right], \quad (5)$$

where f_{rf} is the desired, difference frequency ($f_{tun} - f_{ref}$), and all higher frequency terms have been assumed negligible. Figure 1 (c) illustrates (5) in both time and frequency.

Once the PD generates the RF pulse, the bias tee filters the signal such that only the second term in (5) travels through the waveguide attenuator and into the harmonic mixer and electronic signal analyzer (ESA). To ensure accurate power measurements, the insertion loss of the RF network from the output of the probe to the output of the attenuator was measured, as well as the conversion loss from the mixer to the ESA. In addition to RF losses, the signal experiences pulse

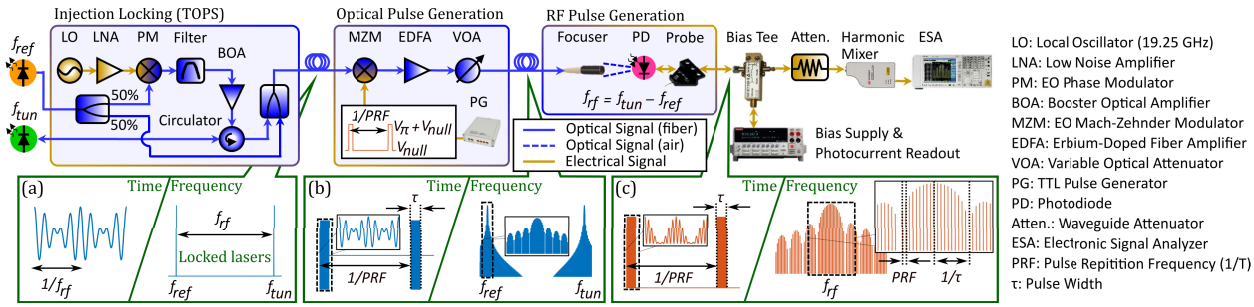

Fig. 1. RF photonic pulse generation system. (a)–(c) Call-outs illustrating expected signal characteristics. Key definitions provided.

desensitization due to the Fourier transform process that takes place in the ESA [14]. This pulse desensitization relates the power displayed at $f = f_{rf}$ for a PW signal to the power that would be displayed at $f = f_{rf}$ for the CW equivalent. In this way, the CW equivalent can be thought of as the signal captured only during the pulse width. Consequently, the CW equivalent power represents the PW peak power. Therefore, if a PW signal is measured with the ESA, the pulse desensitization can be used to determine its peak power, and subsequently its average power.

III. Results

PW measurements were taken at 77 GHz with a pulse period of 1 μs (PRF = 1 MHz) and varying δ. The minimum δ was 0.5 %, corresponding to a pulse width of 5 ns. All PW data was captured using the system shown in Fig. 1 and 8-μm diameter CC-MUTC PDs designed by the University of Virginia [10] and fabricated and tested by the first author. Optical coupling conditions were such that the average responsivity was 0.08 A/W, approximately 50 % of its maximum. This defocusing is a technique employed for surface-illuminated PDs that is believed to improve power handling by promoting lower peak-to-average photocurrent densities [15].

The peak PD output power was calculated following:

$$P_{pk}(dBm) = P_{ESA} + L_{rf} - 20log_{10}(\delta), \tag{6}$$

where P_{ESA} is the measured power, L_{rf} is the RF insertion loss from the probe to the ESA, which was 35.9 dB at 77 GHz, and the expression $20log_{10}(\delta)$ represents the pulse desensitization discussed in Section II. The RF insertion loss was dominated by the waveguide attenuator that was inserted to protect the measurement devices; excluding this, the RF loss was 6.9 dB. The average PD output power was calculated following:

$$P_{av}(dBm) = P_{pk} - 10log_{10}(\delta). \tag{7}$$

Figure 2 (a) shows the maximum measured PD peak and average output powers as a function of δ. As shown, the observed trends in peak and average PD output power are reciprocal and exponential with changes in δ. The dotted lines in Fig. 2 (a) were calculated following a log scale of:

$$P_{pk}(W) = P_{cw}(\sqrt{\delta})^{-1} \quad \text{and} \quad P_{av}(W) = P_{cw}\sqrt{\delta}, \tag{8}$$

where P_{cw} was the maximum PD output power measured during CW operation. Accordingly, it was observed that the peak PD output power could be increased under PW conditions proportional to $1/\sqrt{\delta}$. This led to peak power improvement

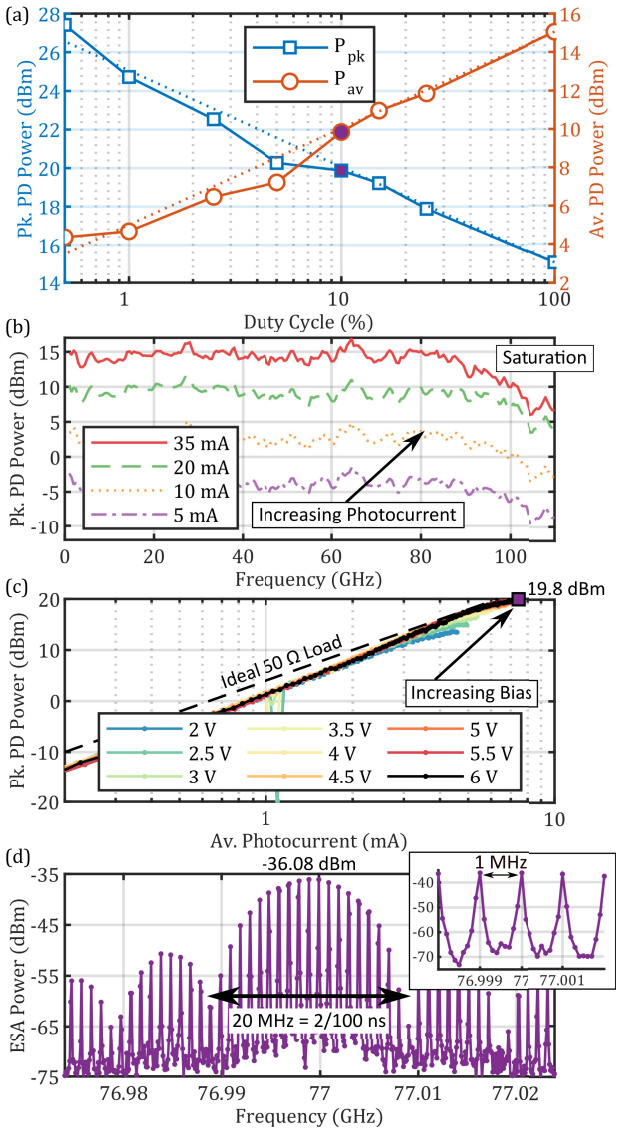

Fig. 2. (a) PW power as a function of δ, (b) CW power as a function of f_{rf}, (c) PW power as a function of I_{av} for $\delta = 10$ %, and (d) ESA trace for $\delta = 10$ %. PW data taken with PRF = 1 MHz and $f_{rf} = 77$ GHz.

upward of 1000 % with $\delta < 1$ %. However, as the peak power improved, the average power degraded. The average power decreased by more than 90 % with $\delta < 1$ %, a relationship that warrants further investigation, as it may be possible to increase the achieved average power by further increasing the peak power with an optimized PD design [7].

The observed improvement in peak PD output power can be explained by PW operation enabling increased saturation

TABLE II
SIGNAL CHARACTERISTICS AT MAXIMUM

τ (ns)	δ (%)	I_{av} (mA)	P_{av} (dBm)	I_{pk} (mA)	P_{pk} (dBm)	Reverse Bias (V)
5	0.5	1.5	4.4	300	27.4	9
10	1	2.1	4.7	210	24.7	9
25	2.5	2.8	6.5	112	22.5	8
50	5	5.2	7.3	104	20.3	6.5
100	10	7.7	9.9	77	19.8	6
150	15	10.5	11	70	19.2	5.5
250	25	14.5	11.9	58	17.9	5
1000	100	35	15.1	35	15.1	4

levels that would otherwise cause thermal runaway and device failure. Figure 2 (b) shows the PD output power during CW operation. For these measurements, the reverse bias was held constant (4 V), f_{rf} was varied, and each curve represents a different I_{av}. As shown, PD response above 80 GHz shows signs of saturation at 35 mA, indicated by the enhanced frequency rolloff. CW operation failed above 4 V for this photocurrent and limited PD output power. Figure 2 (c) shows the PD output power during PW operation with $\delta = 10$ %. For these measurements, f_{rf} was held constant (77 GHz), I_{av} was varied, and each curve represents a different reverse bias. As shown, PD saturation was pushed to higher and higher photocurrent as the reverse bias was increased. This behavior is commonly attributed to space charge resulting from the field imposed by the photogenerated carriers opposing the field imposed by the applied reverse bias. As more carriers are generated (*higher photocurrent*), there exists more opposition to displacement current, and thus more reverse bias is required to maintain linearity. In the absence of saturation, frequency dependence, and laser imbalance, the expected PD output power during PW operation can be expressed as:

$$P_{ideal} = \frac{1}{2} I_{pk}^2 R_{load}, \tag{9}$$

where $I_{pk} = I_{av}/\delta$, I_{av} is the time average of I_{ph} in (5), and R_{load} is the resistance across which the power is measured. Following (9), an increase in peak photocurrent, provided by an increase in reverse bias voltage, will manifest as an increase in maximum PD output power. This relationship was observed as δ decreased and is summarized by Fig. 2 (a) and Table II.

To verify expected pulse characteristics, Fig. 2 (d) shows the trace captured from the ESA during the maximum power measurement with $\delta = 10$ %. The trace captured was consistent with the expected signal behavior as illustrated in Fig. 1. Specifically, the bandwidth occupied by the central lobe is 20 MHz, which is twice the expected bandwidth from the center frequency to the first null as dictated by the reciprocal of $\tau = 100$ ns. In addition to the bandwidth of the central lobe, the PRF is also consistent with the expected value of 1 MHz, as shown by the Fig. 2 (d) inset.

IV. SUMMARY

Record-high W-band photonic pulsed power generation was demonstrated using a widely tunable optical heterodyne system with a high-speed, high-power PD. System architecture was described and PD output power as a function of duty cycle for a 1 MHz PRF was presented. A peak PD output power of 27.4 dBm was measured at 77 GHz for a duty cycle of 0.5 %. To the best of our knowledge, this is the highest reported output power for a W-band PD and a W-band photonic system. Not only does this result support the ongoing effort to improve PD power generation, but it complements the inherent benefits of ultrawide bandwidth and tunability that photonic pulse generation systems can provide.

ACKNOWLEDGMENT

The authors would like to thank JC Campbell (University of Virginia) and collaborators, as well as the team at Phase Sensitive Innovations, Inc., who made this work (AFRL-2022-1296) possible. The views and conclusions contained herein are those of the authors and should not be interpreted as necessarily the official policies or endorsements, either expressed or implied, of Air Force Research Laboratory, the Department of Defense, or the U.S. Government.

REFERENCES

[1] J. Hasch, E. Topak, R. Schnabel, T. Zwick, R. Weigel, and C. Waldschmidt, "Millimeter-wave technology for automotive radar sensors in the 77 GHz frequency band," *IEEE Trans. Microw. Theory Techn.*, vol. 60, no. 3, pp. 845–860, Sep. 2012.

[2] S. Pan and Y. Zhang, "Microwave photonic radars," *J. Lightw. Technol.*, vol. 38, no. 19, pp. 5450–5484, May 7, 2020.

[3] Y. Li, A. Rashidinejad, J.-M. Wun, D. E. Leaird, J.-W. Shi, and A. M. Weiner, "Photonic generation of W-band arbitrary waveforms with high time-bandwidth products enabling 3.9 mm range resolution," *Optica*, vol. 1, no. 6, pp. 446–454, 2014.

[4] M. I. Skolnik, *Introduction to RADAR Systems*. New York, NY, USA: McGraw-Hill, 2001.

[5] A. Kuriyama *et al.*, "High efficiency and small antenna with horn and lens for 77 GHz automotive radar," in *Proc. 18th Int. Symp. Antenna Technol. Appl. Electromagn. (ANTEM)*, Aug. 2018, pp. 1–2.

[6] G. Serafino, F. Amato, S. Maresca, L. Lembo, P. Ghelfi, and A. Bogoni, "Photonic approach for on-board and ground radars in automotive applications," *IET Radar, Sonar Navigat.*, vol. 12, no. 10, pp. 1179–1186, Oct. 2018.

[7] Y. Peng *et al.*, "Photonic generation of pulsed microwave signals in the X-, Ku- and K-band," *Opt. Exp.*, vol. 28, no. 19, pp. 28563–28572, Sep. 2020.

[8] X. Xie *et al.*, "Photonic generation of high-power pulsed microwave signals," *J. Lightw. Technol.*, vol. 33, no. 18, pp. 3808–3814, Sep. 15, 2015.

[9] T. Ishibashi, S. Kodama, N. S. N. Shimizu, and T. F. T. Furuta, "High-speed response of uni-traveling-carrier photodiodes," *Jpn. J. Appl. Phys.*, vol. 36, no. 10, p. 6263, Oct. 1997.

[10] Q. Li *et al.*, "High-power flip-chip bonded photodiode with 110 GHz bandwidth," *J. Lightw. Technol.*, vol. 34, no. 9, pp. 2139–2144, May 1, 2016.

[11] X. Xie *et al.*, "Improved power conversion efficiency in high-performance photodiodes by flip-chip bonding on diamond," *Optica*, vol. 1, no. 6, pp. 429–435, Dec. 2014.

[12] T.-F. Tseng *et al.*, "High-depth-resolution 3-dimensional radar-imaging system based on a few-cycle W-band photonic millimeter-wave pulse generator," *Opt. Exp.*, vol. 21, no. 12, pp. 14109–14119, Jun. 2013.

[13] G. J. Schneider, J. A. Murakowski, C. A. Schuetz, S. Shi, and D. W. Prather, "Radiofrequency signal-generation system with over seven octaves of continuous tuning," *Nature Photon.*, vol. 7, pp. 118–122, Feb. 2013.

[14] *Spectrum and Signal Analyzers Pulsed RF*, Agilent, Santa Clara, CA, USA, Appl. Note 150-2, 1971, pp. 6–9.

[15] K. J. Williams and R. D. Esman, "Design considerations for high-current photodetectors," *J. Lightw. Technol.*, vol. 17, no. 8, pp. 1443–1454, Aug. 1999.